

# Reduced Order Models for Boundary Feedback Flow Control

Seddik M. Djouadi, R.C. Camphouse and J.H. Myatt

**Abstract** -- This paper deals with the practical and theoretical implications of model reduction for aerodynamic flow based control problems. Various aspects of model reduction are discussed that apply to Partial Differential Equation (PDE) based models in general. Specifically, the Proper Orthogonal Decomposition (POD) of a high dimension system as well as frequency domain identification methods are discussed for initial model construction. Projections on the POD basis give a Galerkin model. Then, a model reduction method based on empirical balanced truncation is developed and applied to the Galerkin model. The proposed empirical balanced truncation uses the Galerkin model with a chirp signal as input to produce the output in the Eigensystem Realization Algorithm (ERA). This method estimates the system's Markov parameters that accurately reproduce the output. Then, balanced truncation is used to show that model reduction is still effective on ERA produced approximated systems. The linear empirical balanced truncation algorithm is applied to the Galerkin model which is nonlinear. The rationale for doing so is that linear subspace approximations to exact submanifolds associated with nonlinear controllability and observability require only standard matrix manipulations utilizing simulation/experimental data. The proposed method is applied to a prototype convective flow on obstacle geometry. A  $H^\infty$  feedback flow controller is designed based on the reduced model to achieve tracking, and then applied to the full order model with excellent performance.

## I. INTRODUCTION

Recently there has been significant interest in model reduction for the purpose of control design [2, 3, 12, 15, 16], [19][30][31]. One such application of reduced order modeling is control design in the context of aerodynamic flow. Aerodynamic flow control is a research area of great interest to the Air Force and the fluid mechanics community. Recent advances in the design of actuators and sensors can be leveraged for better system control only if the control design methods provide a reliable low order controller [4]. Additionally, simulation, and experimental diagnostics are making applications such as the suppression of acoustic tones in cavities, and trajectory control without the need to move hinged surfaces a possibility [5].

Reduced models are important for the design of feedback control laws, which rely on models that capture the relevant dynamics of the input-output system and are amenable to control design. In addition, many applications require the integration of feedback control to achieve robustness to

flight condition and vehicle attitude, precision tracking, overcoming low-fidelity models, or moving a system away from a stable solution or limit cycle as efficiently as possible [5]. Unfortunately, it is difficult to create models that capture the relevant dynamics of the input-output system. For example, computational fluid dynamics simulations can provide good solutions to a discretized version of the Navier-Stokes equation [2]. However, accurate simulations for simple shapes such as two-dimensional airfoils, or complex shapes, such as a full vehicle, require several thousands to millions of states. Therefore, the simulation results are not directly useful for control design [5]. The large number of states is necessary to capture important flow features that occur at extremely small spatial scales [4].

POD has been extensively investigated in distributed parameters systems due to its order reduction capability [28]-[31], and balanced truncation, which is a simple yet efficient model reduction technique widely used in reducing model orders of high order linear systems [20], [22], [23]. POD models of only a few dozen states can often accurately capture the input-output behavior of systems that have full order system models of thousands of states [5]. In addition to using the POD method in conjunction with model reduction techniques, the idea of using empirical Gramians is growing in popularity for use in an approximate balanced truncation [14], [15], [27], [9]. Further some work has been done on finding nonlinear empirical Gramians for balanced truncation [6], [9]. However, it might not be possible or practical to actuate over an entire problem region. In the area of fluid mechanics controls must often be fixed to the boundary of the problem geometry. The problem geometry used for this project is one example of a case where control is restricted to the boundaries by physical necessity.

The paper is organized as follows. In Section II we introduce a prototype flow problem geometry that is used to apply the proposed order reduction techniques. Section III introduces empirical balanced truncation. This method is based on approximate (empirical) controllability and observability Gramians and uses only a single simulation/experimental test. Section IV introduces the ERA to identify the Markov parameters of the system, and as a product the empirical Gramians. In Section V, empirical balanced truncation and the ERA algorithm are applied to the Galerkin model, and numerical results are provided to show the effectiveness of the proposed method. An  $H^\infty$  controller based on the empirical reduced model and which achieves tracking is also discussed. The responses of the controlled closed-loop on the full order model are presented, and show that the  $H^\infty$  controller achieves good tracking

<sup>1</sup>S. M. Djouadi, Dept. of Electrical Engineering and Computer Science, University of Tennessee, 1508 Middle Dr., Knoxville, TN 37996, [djouadi@ece.utk.edu](mailto:djouadi@ece.utk.edu).

R.C. Camphouse and J.H. Myatt, are with the Air Force Research Laboratory, Wright-Patterson Air Force Base, Ohio 45433, [russell.camphouse@wpafb.af.mil](mailto:russell.camphouse@wpafb.af.mil), [james.myatt@wpafb.af.mil](mailto:james.myatt@wpafb.af.mil)

performances despite being designed on a much lower model than the original. Section VI contains concluding remarks.

## II. PROBLEM GEOMETRY

The specific problem geometry considered is shown in Figure 1. The problem statement with its corresponding boundary conditions and governing equations was taken from [4]. A realistic example of this geometry in an aerodynamic application would be a payload hatch open during flight with actuator control only on the boundary. Let  $\Omega_{gap}$  be the region defined by  $[a_1, a_2] \times [b_1, b_2]$ . Let  $\Omega_{full}$  be the region defined by  $(a_0, a_{end}) \times (b_0, b_{end})$ . Then the problem domain is given by  $\Omega = \Omega_{full} \setminus \Omega_{gap}$ . In this problem setup,  $\Omega_{gap}$  is an obstacle. The system dynamics that act within the problem domain are described by the two dimensional Burgers' equation [4]:

$$\frac{\partial}{\partial t} w(t, x, y) + \nabla \cdot F(w) = \frac{1}{r} \left( \frac{\partial^2}{\partial x^2} w(t, x, y) + \frac{\partial^2}{\partial y^2} w(t, x, y) \right) \quad (1)$$

where the form of  $F(w)$  is

$$F(w) = \begin{bmatrix} c_1 \frac{w^2(t, x, y)}{2} & c_2 \frac{w^2(t, x, y)}{2} \end{bmatrix}^T \quad (2)$$

In this case, the value for  $c_1$  is equal to 1 and  $c_2$  is equal to 0. The parameter  $r$  controls how much nonlinearity is present in the problem. The value used is 300, a small "Reynolds number" but it still allows for the nonlinearity to show in the problem. Dirichlet boundary conditions [13] located on the obstacle top and bottom are denoted by  $\Gamma_{top}$  and  $\Gamma_{bottom}$ . The form of the boundary condition is

$$w(t, x, y) = f(t, x, y) \quad \forall (x, y) \in \partial\Omega \quad (3)$$

The boundary conditions on the top and bottom are described by the following equations

$$w(t, \Gamma_{bottom}) = u_{bottom}(t) \Psi_{bottom}(x) \quad (4)$$

$$w(t, \Gamma_{top}) = u_{top}(t) \Psi_{top}(x) \quad (5)$$

Here  $u_{top}(t)$  and  $u_{bottom}(t)$  are control inputs on the top and bottom boundaries respectively, the spatial functions  $\Psi_{top}(x)$  and  $\Psi_{bottom}(x)$  describe the spatial effects.

The boundary condition on the airflow intake side is

$$w(t, \Gamma_{in}) = f(y) \quad (6)$$

and it is parabolic in nature. The airflow outtake side has a Neumann boundary condition that has the form [13]

$$\frac{\partial}{\partial x} w(t, \Gamma_{out}) = 0 \quad (7)$$

On all of the remaining boundaries of  $\Omega$ ,  $w(t, x, y)$  is set equal to 0 for all values of  $t$ . Finally, the initial conditions for the interior are given by

$$w(0, x, y) = w_0(x, y) \in L^2(\Omega) \quad (8)$$

A numerical solution based on finite difference was found by simulation using a uniformly spaced grid. The resulting system model contains a little more than 2000 states.

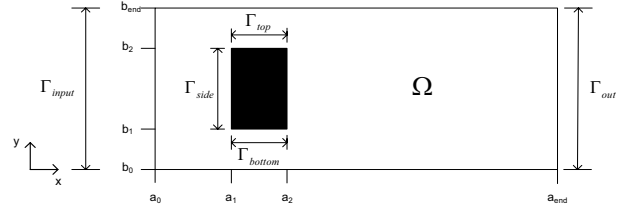


Fig. 1: Problem Geometry

The POD model construction is based on the total energy captured. A condition that 99.9% of system energy must be captured was used for determining how many system modes were retained. This condition was met by a 40 POD basis. Although this is a major reduction from the numerical solution, it will be shown that important system dynamics can be retained with even lower state number system models.

The general approach of this method is to construct a series of solution "snapshots." These snapshots are generated by numerical simulations with a variety of input equations [10, 19]. These inputs should be similar to the expected inputs of the real system. The inputs used here are of the form [4]

$$u_{bottom}(t) = \beta \sin(0.25t^2) \quad u_{top}(t) = 0 \quad (9)$$

$$u_{bottom}(t) = 0 \quad u_{top}(t) = \beta \sin(0.25t^2) \quad (10)$$

$$u_{bottom}(t) = \beta \sin(0.25t^2) \quad u_{top}(t) = \beta \sin(0.25t^2) \quad (11)$$

where the values for  $\beta$  are  $-3$ ,  $-2$ , and  $-1$  and the range for  $t$  is 0 to 10 seconds with a sample every 50 milliseconds. The squelch signal for all three values of  $\beta$  is shown in Figure 2. The numerical simulation was performed to create the ensemble of solution snapshots  $\{S_k(x, y)\}_{k=1}^M$  [4]. The value for  $M$  must be greater than the number of modes that one will choose for the approximated system model [4].

The solution to the PDE is assumed to belong to the  $L^2([0, T] \times \Omega)$ , and can be approximated as

$$w(t, x, y) \approx \sum_{k=1}^n \alpha_k(t) \phi_k(x, y) \quad (12)$$

where the  $\alpha_k$ 's are time varying coefficients that multiply the spatial functions  $\phi_k$ 's and

$\alpha_k \in L^2([0, T])$ ,  $\phi_k(x, y) \in L^2(\Omega)$  where  $L^2([0, T])$  and  $L^2(\Omega)$  are the standard Hilbert spaces of absolutely square integrable functions defined, respectively, on the time interval  $[0, T]$  and spatial domain  $\Omega$ . The approximation (13) can be as accurate as desired since the tensor space

$$L^2([0, T]) \otimes L^2(\Omega) := \left\{ \sum_{k=1}^n \alpha_k(t) \phi_k(x, y), \alpha_k(t) \in L^2([0, T]), \phi_k(x, y) \in L^2(\Omega), \forall n \text{ integer} \right\} \text{ is}$$

dense in  $L^2([0, T] \times \Omega)$  [14]. Any basis for  $L^2(\Omega)$  can be used to construct the approximation of the solution  $w(t, x, y)$ . Here we use the POD basis  $\{\phi_k\}$  since it is optimal in the following sense [3]

$$\mu_n := \inf_{\substack{\alpha_k \in L^2([0, T]), \\ \phi_k(x, y) \in L^2(\Omega)}} \left\| w(t, x, y) - \sum_{k=1}^n \alpha_k(t) \phi_k(x, y) \right\|_2$$

$$\mu_n \xrightarrow{n \rightarrow \infty} 0$$

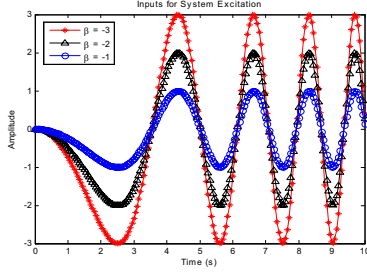


Fig. 2: Test Inputs Used to Generate the Snapshots

In [3] it is shown that solving the above optimization reduces to the usual POD optimality in the average kinetic energy sense (19) discussed below [10]. The POD basis function  $\varphi_i$  is chosen to maximize the average projection of

$$\text{the member } u_i \text{ onto } \varphi_i, \quad \max_{\varphi_i \in L^2(\Omega)} \frac{\langle u_i, \varphi_i \rangle^2}{\|\varphi_i\|_2^2} \quad [10].$$

To construct numerically the POD basis  $\{\varphi_j\}$ , we build the correlation matrix  $L$ , of size  $M \times M$ , composed of the inner products of the snapshots. In  $L^2(\Omega)$  we have

$$L_{k,j} = \langle S_k, S_j \rangle \quad \langle S_k, S_j \rangle = \int_{\Omega} S_k S_j^* dx dy \quad (13)$$

where  $*$  denotes complex conjugate transpose. A singular value decomposition of the matrix  $L$  is performed. The  $n$  largest eigenvalues  $\{\lambda_1, \lambda_2, \dots, \lambda_n\}$  of the matrix  $L$  are found and placed in descending order. Then the set of eigenvectors  $\{v_1, v_2, \dots, v_n\}$  are identified. The resulting orthonormal POD basis  $\{\varphi_j\}$  of dimension  $n$  can be constructed using the information found from the correlation matrix  $L$ . First, the eigenvectors of  $L$  are weighted by their corresponding eigenvalues and normalized according to [4]

$$\lambda_k \|v_k\|^2 = 1, \text{ for } k = \{1, 2, \dots, n\}. \quad (14)$$

Then, the POD basis set is formed according to

$$\varphi_k(x, y) = \sum_{j=1}^M v_{k,j} S_j(x, y) \quad (15)$$

with  $v_{k,j}$  being the  $j^{\text{th}}$  component of the eigenvector  $v_k$ .

with  $v_{k,j}$  being the  $j^{\text{th}}$  component of the eigenvector  $v_k$ . Solving equation (21) gives  $n$   $\varphi_k$ 's, which constitute the POD basis of dimension  $n$ . The governing equation is projected onto the POD basis. The projection is accomplished via a Galerkin type projection. The Galerkin projection results in only a weak solution to the PDE. However, this weak solution with finite difference approximations of the boundary conditions eventually leads to a nonlinear temporal model for the temporal or POD coefficients  $\{\alpha_k\}$  [4]

$$\dot{\alpha} = A\alpha + Bu + N(\alpha) + F, \quad \alpha(0) = \alpha_o$$

where  $\alpha \in \mathbb{R}^n$  and the matrices  $A$  is  $n \times n$ ,  $B$  is  $n \times 2$ ,  $N$  and  $F$  are both vectors  $n \times 1$ . The output equation will be simply chosen to be

$$y(t) = \alpha(t)$$

In this model the dimension of the state vector  $\alpha$  is 40 which correspond to 40 POD modes. The first 8 POD modes corresponding to the first 8 temporal coefficients are shown in Figure 3. The first model corresponds to the baseline mode, and the remaining modes to actuated modes. To test the validity of the POD model the following test inputs applied at the boundary are used

$$u_1(t) = \sin\left(\frac{3\pi t}{4}\right) \quad u_2(t) = \sin\left(\frac{3\pi t}{2}\right)$$

In Figure 4, dashed lines denote the linear combination of POD modes restricted to the boundary. Solid lines denote the boundary test inputs. As can be seen in Figure 4, there is very good agreement between the boundary conditions specified for the full order system and the linear combination of POD modes restricted to the boundary.

The goal of model reduction is to construct another nonlinear system [4][5]

$$\dot{\alpha}_r = A_r \alpha_r + B_r u + N_r(\alpha_r) + F_r \quad (16)$$

where  $\alpha_r \in \mathbb{R}^r$  and  $r < n$ , such that the behavior of the two systems is similar for states in some region of the state space. The reduced model is derived via the construction of an immersion/projection pair

$$\alpha = \tilde{T} \alpha_r \quad \alpha_r = T \alpha \quad T \tilde{T} = I_r \quad (17)$$

where  $I_r$  is the  $r \times r$  identity matrix, resulting in the following reduced model

$$\dot{\alpha}_r = T A \tilde{T} \alpha_r + T B u + T N(\tilde{T} \alpha_r) + T F, \quad y(t) = C \tilde{T} \alpha_r(t) \quad (18)$$

This is carried out by developing an empirical balanced truncation algorithm which is based on experimental/simulation input-output measurements of the nonlinear Galerkin model. To do so we need first to introduce the balanced truncation model reduction.

### III. EMPIRICAL BALANCED TRUNCATION

The dynamics of (finite dimensional) LTI systems are governed by a state space model of the form

$$G: \dot{x}(t) = Ax(t) + Bu(t) \\ y(t) = Cx(t) + Du(t) \quad (19)$$

where  $x(t) \in \mathbb{R}^n$  is the state vector,  $u(t) \in \mathbb{R}^m$  is the input, and  $y(t) \in \mathbb{R}^p$  is the output. The first step in applying balanced truncation is to compute a coordinate transformation  $M$  such that the controllability and observability Gramians, denoted  $W_c$  and  $W_o$  respectively, of the system are equal and diagonal.

A balanced realization needs a similarity transformation  $M$  such that the transformed Gramians are equal and satisfy [22][23][27]

$$\hat{W}_o = \Sigma = \hat{W}_c \quad (20)$$

where the matrix  $\Sigma$  is a diagonal matrix containing constants in monotonically decreasing order.

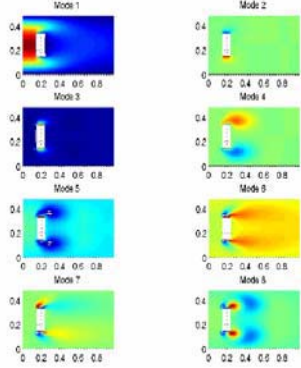


Fig. 3: First Eight POD modes

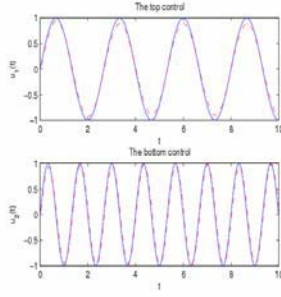


Fig. 4: Boundary Control Accuracy

For a system with  $n$  states, the controllability and observability matrices are  $n \times n$  symmetric and therefore solving for each one of them involve finding  $n$  unknowns. An alternative is to develop a balanced truncation algorithm based on empirical Gramians, which are constructed solely from a single simulation/experiment using a sufficiently rich input. To this end, let us first introduce the  $l$ -step observability and  $q$ -step controllability matrices [20]

$$O_l := \begin{bmatrix} C^T & (CA)^T & \dots & (CA^{l-1})^T \end{bmatrix}^T, R_q := \begin{bmatrix} B & AB & \dots & A^{q-1}B \end{bmatrix}$$

which give rise to the  $l$ -step observability and  $q$ -step controllability Gramians  $W_{ol} := O_l^* O_l$ ,  $W_{cq} := R_q R_q^*$ .

As the numbers  $q$  and  $l$  approach infinity, these empirical Gramians approach the true Gramians

$$\lim_{l \rightarrow \infty} W_{ol} = W_o, \lim_{q \rightarrow \infty} W_{cq} = W_c \quad (21)$$

The goal is to find a balancing transformation matrix  $M$  that will approximately balance the empirical Gramians, i.e.,

$$\hat{W}_{cq} := M W_{cq} M^* = (M^*)^{-1} W_{ol} M^{-1} =: \hat{W}_{ol} = \Sigma \quad (22)$$

The matrix  $M$  can then be applied back to the original system model to produce an approximately balanced realization. The product of the  $l$ -step controllability and the and the  $q$ -step observability matrices gives a Hankel<sup>1</sup> matrix, denoted  $H_{lq}$ , containing the Markov parameters  $CA^k B$ ,  $k = 0, 1, \dots$ , of the system in the following way

$$H_{lq} := O_l R_q = \begin{bmatrix} CB & CAB & \dots & CA^{q-1}B \\ CAB & CA^2B & \dots & CA^qB \\ \vdots & \vdots & \ddots & \vdots \\ CA^{l-1}B & CA^lB & \dots & CA^{l+q-2}B \end{bmatrix} \quad (23)$$

for integers  $l$  and  $q$  chosen such that [20]

$$\text{rank}(H_{lq}) = \text{rank}(H_{(l+1)(q+j)}) = n, \quad \forall j \geq 1 \quad (24)$$

In terms of the SVD decomposition of  $H_{lq}$

<sup>1</sup> A Hankel matrix when considered in block form is simply a matrix that has the  $i^{\text{th}}$  column identical to the  $i^{\text{th}}$  row.

$$H_{lq} = U \Sigma V^* = \begin{bmatrix} U_1 & U_2 \end{bmatrix} \begin{bmatrix} \Sigma_1 & 0 \\ 0 & 0 \end{bmatrix} \begin{bmatrix} V_1^* \\ V_2^* \end{bmatrix} \quad (25)$$

The balancing transformation  $M$  is constructed as [15]  $M = R_q V_1 \Sigma_1^{-1/2}$ . A straightforward computation shows

$$\hat{W}_{cq} := M^{-1} W_{cq} M^{*-1} = M^* W_{ol} M =: \hat{W}_{ol} = \Sigma_1 \quad (26)$$

Balanced truncation can be realized the usual way, if  $\sigma_r \gg \sigma_{r+1}$  for some  $r$  then we can partition  $\Sigma_1$  as

$$\Sigma_1 = \text{diag}(\Sigma_r, \Sigma_{r+1}) \quad (27)$$

where

$$\Sigma_r = \text{diag}(\sigma_1, \sigma_2, \dots, \sigma_r), \Sigma_{r+1} = \text{diag}(\sigma_{r+1}, \sigma_{r+2}, \dots, \sigma_n)$$

A columnwise conformal partition of  $U_1$  and  $V_1$

$$U_1 = [U_r \ U_{n-r}], \quad V_1 = [V_r \ V_{n-r}] \quad (28)$$

yields the immersion/projection pair [15]

$\tilde{T}_r = R_q V_r \Sigma_r^{-1/2}$ ,  $T_r = \Sigma_r^{-1/2} U_r^* O_l$ ,  $T_r \tilde{T}_r = I_r$  and from which a reduced order  $r$ -dimensional model with state matrices is deduced

$$A_r = T_r A \tilde{T}_r, \quad B_r = T_r B, \quad C_r = C \tilde{T}_r \quad (29)$$

The above construction only requires estimates of the Markov parameters  $CA^k B$ ,  $k = 0, 1, \dots, l+q-1$ .

A basic relationship between the Markov parameters and the input and output relationship in discrete-time is

$$y(k) = \sum_{\ell=0}^{\infty} Y(\ell) u(k-\ell) \quad (30)$$

$$Y(0) = D, \quad Y(1) = CB, \dots, \quad Y(k) = CA^{k-1}B \quad (31)$$

The Markov parameters can be computed from a single simulation/experiment in which a sufficiently rich input signal is applied and the output responses are collected. In the next section, the Discrete Fourier Transform (DFT) is used to map time domain data into spectral densities from which frequency response estimates are calculated using the Eigensystem Realization Algorithm (ERA) [25].

#### IV. EIGENSYSTEM REALIZATION ALGORITHM

Several frequency domain identification techniques are used in practice to identify the model parameters. One such method is the ERA technique [25] and is applied to discrete time versions of system models.

An alternative form to (30) can be created not using the actual outputs and inputs but replacing the output term by the cross-correlation between the inputs and the corresponding outputs

$$R_{yu}(k) = \sum_{\ell=0}^{\infty} Y(\ell) R_{uu}(k-\ell) \quad (32)$$

where the length of the data sequence is

$$R_{uu}(k) = \frac{1}{m} \sum_{\tau=0}^{m-1} u(\tau) u^T(k-\tau), \quad R_{yu}(k) = \frac{1}{m} \sum_{\tau=0}^{m-1} y(\tau) u^T(k-\tau) \quad (33)$$

The basic process for finding the Markov parameters starts using the ratio of the power spectral density of the cross-

correlation between the inputs and outputs and the power spectral density of the autocorrelation between the input signals. These power spectral densities are

$$P_{yu}(k) = \frac{1}{m} \sum_{\tau=0}^{m-1} R_{yu}(\tau) e^{-j\frac{2\pi k}{m}\tau}, P_{uu}(k) = \frac{1}{m} \sum_{\tau=0}^{m-1} R_{uu}(\tau) e^{-j\frac{2\pi k}{m}\tau} \quad (34)$$

The ratio of the two power spectral densities is the frequency response function, denoted,  $G(z_k)$ . Then, the final step is to take the inverse Fourier transform to find the pulse response (Markov parameter) matrices [25]

$$Y_k := Y(k) = \sum_{\ell=0}^{\infty} G(z_k) e^{j\left(\frac{2\pi\ell}{m}\right)k} \quad (35)$$

The Hankel matrix containing the Markov parameters is of the following form

$$H_{lq} = \begin{bmatrix} Y_1 & Y_2 & \cdots & Y_q \\ Y_2 & Y_3 & \cdots & Y_{q+1} \\ \vdots & \vdots & \vdots & \vdots \\ Y_l & Y_{l+1} & \cdots & Y_{q+l-1} \end{bmatrix} \quad (36)$$

The individual  $Y_k$ 's correspond to the following sequence

$$Y_0 = D, Y_1 = CB, \dots, Y_k = CA^{k-1}B \quad (37)$$

In some cases the input data for the ERA method might be provided by an experiment on a real system. However, in this paper a unique approach of using the Galerkin model in the place of the real system was used to generate the empirical data. The full order system model was created using finite-difference methods. Recall that the control inputs were explicitly placed in the boundary conditions, because the control inputs do not show up explicitly in the two-dimensional Burgers' equation. However, the weak Galerkin model results in a nonlinear state space model that simplifies the relationship between the input and outputs. The chirp signals used for the excitation of the Galerkin model are of the following form and are shown in Figure 5.

$$u_1(t) = -\sin(0.55t^2) \quad u_2(t) = -\sin(0.60t^2) \quad (38)$$

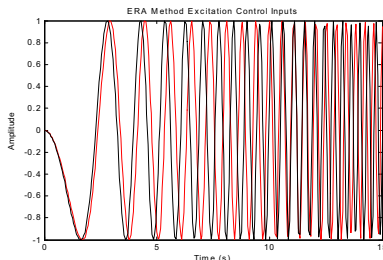


Fig. 5: Excitation Inputs for ERA Method

## V. APPLICATION TO THE GALERKIN MODEL

The empirical balanced truncation based on linear systems is applied to the Galerkin model

$$\dot{\alpha} = A\alpha + Bu + N(\alpha) + F, \quad \alpha(0) = \alpha_o \quad (39)$$

which has an equilibrium in steady state, denoted by  $\alpha_{ss}$ .

The rationale for doing so is that linear subspace approximations to exact submanifolds associated with nonlinear controllability and observability require only standard matrix manipulations utilizing simulation/

experimental data, denoted by  $\alpha_{ss}$ . The rationale for doing so is that linear subspace approximations to exact submanifolds associated with nonlinear controllability and observability require only standard matrix manipulations utilizing simulation/experimental data as explained in [15,36,37]. The computational advantages of the scheme presented here carry over directly to the nonlinear setting. The reduced order model is derived as discussed through the construction of the immersion/projection nonlinear system pair  $\alpha = \tilde{T}\alpha_r, \alpha_r = T\alpha$ . This results in the following reduced-order model

$$\dot{\alpha}_r = A_r\alpha_r + B_ru + N_r(\tilde{T}\alpha_r) + F_r, \quad \alpha_r(0) = T\alpha_o \quad (40)$$

$$A_r := TA_r\tilde{T}, B_r := TB, N_r := TN, F_r := TF$$

If (39) has a linearization around  $\alpha_{ss}$

$$\dot{\alpha} = A_t\alpha + B_tu, \quad \alpha(0) = \alpha_o \quad (41)$$

and the reduced system linearization is

$$\dot{\alpha}_r = A_{tr}\alpha_r + B_{tr}u, \quad \alpha_r(0) = T\alpha_o \quad (42)$$

The linearization of both models are related by

$$A_{tr} = TA_t\tilde{T}, B_{tr} = TB_t$$

Empirical balanced truncation applied to the 40<sup>th</sup> order Galerkin model resulted in a 14<sup>th</sup> order reduced models. The first 8 temporal coefficients of the 14<sup>th</sup> order reduced model and 2000<sup>th</sup> full order model are plotted in Figure 6.

In Figure 7, we compare the Hankel singular values of the 2000<sup>th</sup> full order linearized and reduced 14<sup>th</sup> order empirical model. As expected the Hankel singular values corresponding to the reduced order model are smaller than the full order model, nevertheless the Figure shows that they are close. In Figure 8 we compare the full order solution  $w(t, x, y)$  of the Burgers' equation with the solution based on the 14 order ERA model  $w_r(t, x, y)$ . The Figure shows that they behave similarly especially at the boundary where control is applied.

An  $H^\infty$  controller was designed based on the linearized 14<sup>th</sup> order reduced model and applied to the full order model using Matlab. The performance was to achieved tracking a fixed reference signal  $w_{ref}(x)$  specified for the full order model (see [5] for the details). Projecting  $w_{ref}(x)$  onto the POD basis yields tracking coefficients for the reduced order model. After computing the  $H^\infty$  controller we close the loop on the original 2000<sup>th</sup> full order model. The controller is only 14<sup>th</sup> order since based on the 14<sup>th</sup> order reduced model. The projected reference onto the POD basis initial condition and reference are shown in Figure 9. The controlled flow with the action of the boundary controller is shown in Figure 10. The Figure shows good tracking performance.

## VI. CONCLUSION

Empirical balanced truncation has been considered in conjunction with POD as an approach for deriving reduced-order models and applied to the 2D Burgers' equation. Like POD, empirical balanced truncation is based on

simulation/experimental data and can be implemented via standard matrix computations. Improvements to the scheme originally proposed in [9, 15] have been presented that lead to reduced data requirements that may become significant for applications such as aerodynamic flow control. Essentially, the balancing transformation is constructed via Markov parameters that can be identified from measurements collected in a single experiment/ simulation. The approach has been applied with favorable results to the 2D Burgers' equation, a partial differential equation in two spatial dimensions that possesses features comparable to the Navier-Stokes equations governing fluid flow. A  $H^\infty$  feedback flow controller was designed based on the empirical reduced model to achieve flow tracking. The closed-loop on the full order model shows good flow tracking performance.

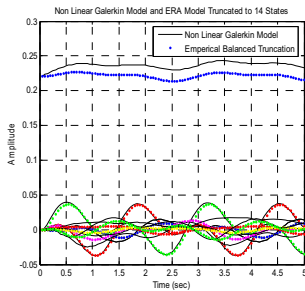


Fig. 6: Projected and POD Model Coefficients

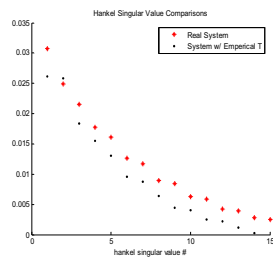


Fig. 7: Comparison of Hankel Singular Values

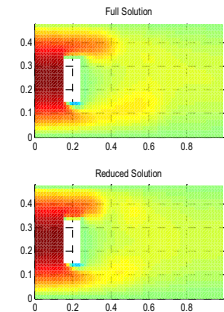


Fig. 8: Full and Reduced Order Models' Responses

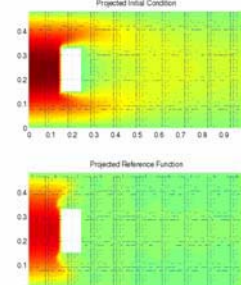


Fig. 9: Initial Flow

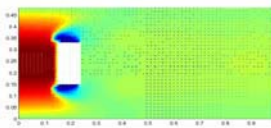


Fig. 10: Controlled Flow

## REFERENCES

[1] Atwell, J. A., Borggaard, J. T., King, B. B., "Reduced Order Controllers For Burgers' Equation With A Nonlinear Observer", *Int. J. Appl. Math. Computational Science.*, 2001, Vol.11, No.6, pgs. 1311-1330.  
 [2] Willcox, K. and Peraire, J., *Balanced Model Reduction via the Proper Orthogonal Decomposition*, AIAA, Vol. 40, No. 11, November 2002, pp. 2323-2330.  
 [3] Djouadi, S.M., R.C. Camphouse and J.H. Myatt, *Optimal Order Reduction for the Two-Dimensional Burgers' Equation*, accepted for presentation in the IEEE Conference on Decision and Control 2007.  
 [4] Camphouse, Chris R. and James H. Myatt, "Reduced Order Modelling and Boundary Feedback Control of Nonlinear Convection", in

American Institute of Aeronautics and Astronautics Guidance, Navigation, and Control Conference, 2005.  
 [5] Camphouse, R. C., Djouadi, S. M., and Myatt, J. H., "Feedback Control for Aerodynamics". IEEE Conference on Decision and Control, Dec 2006.  
 [6] Condon, M. and Ivanov, R., "Empirical Balanced Truncation of Nonlinear Systems," *Journal of Nonlinear Science*. Vol. 14: pp. 405-414, 2004.  
 [7] Efe, M. O. And Ozbay H., "Proper Orthogonal Decomposition for Reduced Order Modeling: 2D Heat Flow," *Proc. Of IEEE CCA*, 2003.  
 [8] Elkin, V. I., *Reduction of Nonlinear Control Systems: A Differential Geometric Approach*, Kluwer Academic Publishers, 1997.  
 [9] Hahn, J. and Edgar, T. F., "Reduction of nonlinear models using balancing of empirical Gramians and Galerkin projections," *Proceedings of the American Control Conference*, June 2000.  
 [10] Holmes, P., Lumley, J. L., Berkooz, G., *Turbulence, Coherent Structures, Dynamical Systems and Symmetry*, Cambridge University Press, 1996.  
 [11] Hui-chuan, S., "Exact Solutions of Navier-Stokes Equations – The Theory of Functions of a Complex Variable Under Dirac-Pauli Representation and its Application in Fluid Dynamics (II)", *Applied Mathematics and Mechanics*, Vol 7. No. 6, June 1986.  
 [12] Ilak, M. and Rowley, C. W., "Reduced-Order Modeling of Channel Flow Using Traveling POD and Balanced POD", *AIAA Flow Control Conference*, 5-8 June 2006.  
 [13] Chung, T. J., *Computational Fluid Dynamics*, Cambridge University Press, 2002.  
 [14] Defant, A and K. Floret, *Tensor Norms and Operator Ideals*, Elsevier Science, 1993.  
 [15] Lawrence, D. A., "Empirical Model Reduction for Active Closed-Loop Flow Control", *Final Report for Faculty Summer Research Opportunity*, ARL Ohio, 2004.  
 [16] Leibfritz, F. and Volkwein, S., "Numerical feedback controller design for PDE systems using model reduction: techniques and case studies". *Real-Time PDE-Constrained Optimization*, SIAM, 2006.  
 [17] Balas, G. J., and Doyle, J. C., "Robustness and Performance Tradeoffs in Control Design for Flexible Structures." *Proceedings of the 29th Conference on Decision and Control*, Honolulu, Hawaii Dec., 1990.  
 [18] Mathworks, "Partial Differential Equations Toolbox Help". Available at <http://www.mathworks.com/access/helpdesk/help/toolbox/pde/>  
 [19] Rowley, C. W., Colonius, T., Murray, R. M., "Model reduction for compressible flows using POD and Galerkin projection." *Physica D*, 189 (2004), pages 115-129.  
 [20] Rugh, W. J., *Linear System Theory*, Prentice Hall, Second Edition, 1996.  
 [21] Sohr, H., *The Navier-Stokes Equations: An Elementary Functional Analytic Approach*, Birkhauser Verlag, 2001.  
 [22] Zhou, K., Doyle, J.C., and Glover, K., *Robust and Optimal Control*, Prentice Hall, 1996.  
 [23] Zhou, K. and Doyle, J. C., *Essentials of Robust Control*, Prentice Hall, 1998.  
 [24] Camphouse, R. C., "Boundary Feedback Control Using Proper Orthogonal Decomposition Models", *Journal of Guidance, Control, and Dynamics*, vol 28, no 5, September-October, 2005.  
 [25] Juang, J., *Applied System Identification*, Prentice Hall, 1994.  
 [26] Tennekes, H. and Lumley, J. L., *A First Course in Turbulence*, The Massachusetts Institute of Technology, 1972.  
 [27] Moore, B. C., "Principal Component Analysis in Linear Systems: Controllability, Observability, and Model Reduction," *Trans. on Automatic Control*, pp. 17-32, 1981.  
 [28] Banks, H., del Rosario, R., and Smith, R., *Reduced Order Model Feedback Control Design: Numerical Implantation in a Thin Shell Model*, Technical Report CRSC-TR98-27, Center for Research in Scientific Computation, North Carolina State University, June, 1998.  
 [29] Caraballo, E., Samimy, M., and DeBonis, J., *Low Dimensional Modeling of Flow for Closed-Loop Flow Control*, AIAA Paper 2003-0059, January 2003.  
 [30] Carlson, H., Glauser, M., Higuchi, H., and Young, M., *POD Based Experimental Flow Control on a NACA-4412 Airfoil*, AIAA Paper 2004-0575, January 2004.  
 [31] Carlson, H., Glauser, M., and Roveda, R., *Models for Controlling Airfoil Lift and Drag*, AIAA Paper 2004-0579, January 2004.